Monte Carlo simulation-based feasibility study of novel indirect flat panel detector system for removing scatter radiation

尹, 湧琇

https://doi.org/10.15017/1866263

出版情報：九州大学, 2017, 博士（保健学）, 課程博士
バージョン：

Physica Medica 32 (2016) 182–187

Contents lists available at ScienceDirect

Physica Medica

journal homepage: http://www.physicamedica.com

Original Paper

Monte Carlo simulation-based feasibility study of novel indirect flat panel detector system for removing scatter radiation

Yongsu Yoon [a], Junji Morishita [b], MinSeok Park [c], Hyunji Kim [d,e], Kihyun Kim [e], Jungmin Kim [e,*]

[a] Department of Health Sciences, Graduate School of Medical Sciences, Kyushu University, Fukuoka 812-8582, Japan
[b] Department of Health Sciences, Faculty of Medical Sciences, Kyushu University, Fukuoka 812-8582, Japan
[c] Radiation Safety Section, Korea Institute of Radiological and Medical Sciences, Seoul 139-706, Republic of Korea
[d] Division of Medical Radiation, Center for Disease Prevention, Korea Centers for Disease Control & Prevention, Chungchongbuk-do 363-700, Republic of Korea
[e] School of Health and Environmental Science, Korea University, Seoul 136-703, Republic of Korea

ARTICLE INFO

Article history:
Received 4 July 2015
Received in revised form 11 November 2015
Accepted 22 November 2015
Available online 4 December 2015

Keywords:
Indirect flat panel detector
Monte Carlo simulation
Scatter radiation

ABSTRACT

The purpose of this study is to investigate the feasibility of a novel indirect flat panel detector (FPD) system for removing scatter radiation. The substrate layer of our FPD system has a Pb net-like structure that matches the ineffective area and blocks the scatter radiation such that only primary X-rays reach the effective area on a thin-film transistor. To evaluate the performance of the proposed system, we used Monte Carlo simulations to derive the scatter fraction and contrast. The scatter fraction of the proposed system is lower than that of a parallel grid system, and the contrast is superior to that of a system without a grid. If the structure of the proposed FPD system is optimized with respect to the specifications of a specific detector, the purpose of the examination, and the energy range used, the FPD can be useful in diagnostic radiology.

Introduction

In plain radiography, the behavior of primary rays from the X-ray tube can be classified according to whether they penetrate without any change in direction, are completely absorbed inside the patient, or interact with the patient and scatter, which is commonly known as scatter radiation or scatter photons [1]. Scatter radiation reaches the detector together with the primary rays and generates an electrical signal in the X-ray detection system, which degrades the image contrast. In a previous study, more than seven times as many scatter photons as incident X-rays were generated in a 20-cm-thick water phantom [2]. There have been many attempts to reduce scatter radiation, and the International Commission on Radiological Protection recommended that in diagnostic radiology, the scatter radiation generated in patients should be removed using a "material with a low attenuation coefficient" [3].

The recent trend in plain radiography is away from film/screen systems and toward digital systems such as storage phosphor systems and indirect/direct flat panel detectors (FPDs) [4]. The grid structure has been used to remove scatter radiation in film/screen systems since the early 1900s [5] and in digital radiography without any new innovative changes except for using a different interspace material and high-density grids. The existing grid system has several shortcomings. First, the shadow of the grid on the detector can cause a grid artifact to appear on the acquired image [6,7]. To avoid this problem, the grid can be moved by motors; however, for a compact system design, a stationary grid system with a high density of 60 lines/cm or more is preferred [8]. The grid pattern caused by grid shadow rarely appeared once the high-density grid began to be used in digital radiography. However, optimization of grid frequency (lines/cm) and of the sampling pitch of the digital radiography system is required to avoid the aliasing artifact [9].

Indirect FPDs have a thin film transistor (TFT) for each pixel size [10]; and hence, the scatter radiation signal would not enter the effective area on the pixel. Therefore, if the Pb in the grid does not block the effective area on the TFT layer, the grid artifact as an aliasing error is not seen. Furthermore, the image quality is improved by adapting the existing grid system, but the exposure dose must be increased to obtain the same image quality. The exposure dose could be reduced if there are no obstructions above the effective area on the pixel, so that the intact effective area is maintained.

We studied the feasibility of a novel CsI-based FPD system with a Pb net-like structure in the substrate layer that matches the

* Corresponding author. School of Health and Environmental Science, Korea University, Seoul 136-703, Republic of Korea. Tel.: +82-2-3290-5685; fax: +82-2-916-5943.
E-mail address: minbogun@korea.ac.kr (J. Kim).

http://dx.doi.org/10.1016/j.ejmp.2015.11.008
1120-1797/

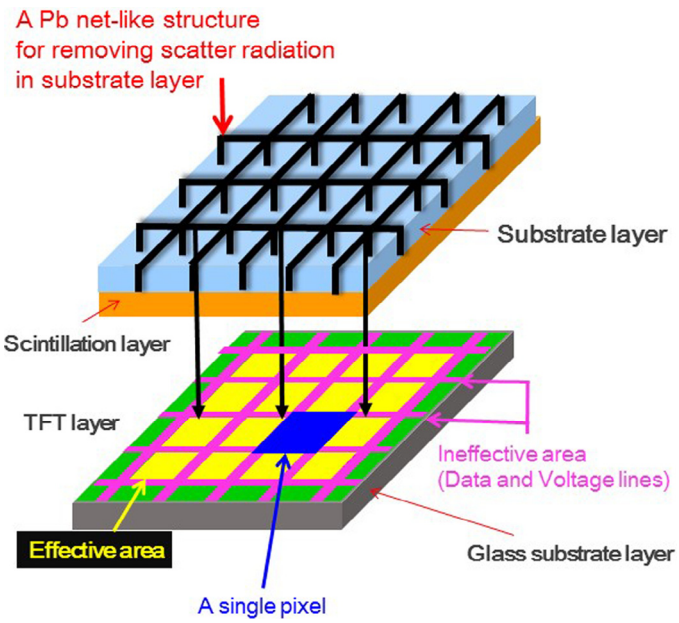

Figure 1. Schematic illustration of the novel CsI-based FPD for removing scatter radiation. (For interpretation of the references to color in this figure legend, the reader is referred to the web version of this article.)

ineffective area and blocks the scatter radiation such that only primary X-rays reach the effective area.

Materials and methods

Concept of the CsI-based indirect FPD system

The indirect FPD comprises three layers: substrate, scintillation layer, and TFT [11]. In most indirect FPDs, there are two different ways to align the scintillation on the top of the CMOS or CCD. One is by direct deposition of the scintillation layer on the CMOS or CCD [12] and the other is by optical coupling of the scintillation layer that is deposited on another substrate such as graphite or an Al plate. Direct deposition is much easier with respect to the fabrication process; however, most manufacturers use the optical coupling technique at present [13]. There have been several studies on the use of the structured scintillation layer in imaging applications [14–16]. Some studies aimed to develop an indirect FPD system with a net-like pixelated CsI scintillation layer meant to enhance spatial resolution and detection efficiency. However, this approach induces scattered light in the scintillation layer. Meanwhile, the TFT layer is a matrix of pixels [17] and ineffective areas where voltage and data lines cross the space between the pixels, and only the effective area of a single pixel can detect the signals [18]. We devised a new FPD system with a Pb net-like structure in the substrate layer that matches the ineffective area in the TFT and blocks the scatter radiation by using the concept of an antiscatter grid so that only primary X-rays reach the effective area (Fig. 1).

Monte Carlo simulation to investigate the feasibility of the FPD system

To investigate the feasibility of our FPD system, we performed Monte Carlo simulations by using MCNPX 2.6.0 software (Los Alamos National Laboratory, Los Alamos, NM, USA) [19]. In addition, SRS-78 software [20] was used to simulate the continuous X-ray spectrum with the following conditions: a tungsten (W) anode, a 12° target angle for the anode, and an additional 0.5-mm-thick copper filter. We calculated the scatter fractions under five simulation conditions: no grid, a parallel grid (Mitaya Manufacturing, Co., Ltd., Saitama, Japan), and three indirect FPD systems. The parallel grid had an 8:1 grid ratio, 60 lines/cm strip density, 0.96-mm-thick Pb septum, and 100-cm focusing distance. Table 1presents the specifications of the three simulated indirect FPD systems. In this simulation study, the substrate layer was graphite ($_{6}C$), the density and thickness of which were 2.15 g/cm^3 and 572 μm, respectively. The scintillation layer was CsI (density: 4.51 g/cm^3, thickness: 600 μm), in which the ratio of $_{55}Cs$ to $_{53}I$ was 1:1. Tally 8 (pulse height tally) was used to record the result of photon absorption in each pixel of the simulated detector; based on the tally option, the energy cutoff was set to 50 eV. The default cross sections of photon interaction were set by using an LCA card and a photon physics card (Phys:P). Because the energy used in this study was in the range of 10–140 keV, a range generally used in diagnostic radiology, we did not modify any physics models in the simulation. Point source radiation was used, and the exposure area was set to cover the entire limited detection area of 2 cm × 2 cm. The source-to-detector distance (SDD) was fixed at 100 cm in all simulation systems. In clinical situations, it is impossible to remove the gap the between the grid and the detector in the parallel grid system. Therefore, for the simulation, we set the air gap between the parallel grid and the detector at 2 cm. The electrons induced by photon interactions were not included as transport particles in this study. In addition, we did not include the results of the simulated optical light photons because this study was about improving the performance of the novel FPD system, not about evaluating the capacity of the CsI used as the scintillation material. The number of histories was controlled to maintain a statistical error <5% [19,21].

Index for evaluating the performance of the novel indirect FPD system: scatter fraction

In diagnostic radiology, the X-rays that reach the detector after passing through the patient consist of a primary component and a scatter radiation component. To investigate the effect of scatter radiation on image quality, it is necessary to determine the values of these two components, I_s and I_p. The effect of scatter radiation on image quality may be in terms of scatter fraction [22]. Scatter fraction is the fraction of total radiation that results from scatter radiation. The performance of the novel indirect FPD system was evaluated using the scatter fraction value. Scatter radiation reduces image contrast, so a low scatter fraction (%) means better image quality. However, it is difficult to measure only the primary or only the scatter radiation under real conditions, although some studies

Table 1
Specifications of three simulated novel indirect FPD systems with different pixel size, thickness of Pb, and effective area of each pixel.

	Simulation #1	Simulation #2	Simulation #3
Matrix size	129 × 129	129 × 129	129 × 129
Total pixel size	153 μm × 153 μm	153 μm × 153 μm	163 μm × 163 μm
Thickness of Pb (ineffective area, μm)	10	20	20
Effective area of each pixel (μm)	143 μm × 143 μm	133 μm × 133 μm	143 μm × 143 μm
Thickness of CsI (μm)	600	600	600

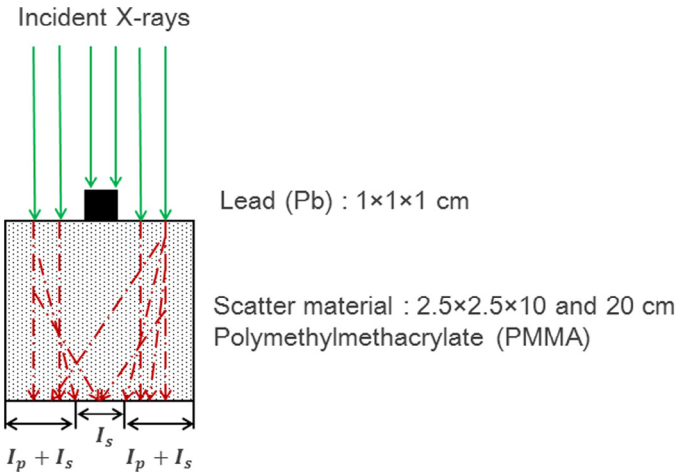

Figure 2. Arrangement of PMMA phantom and Pb cube for measuring scatter radiation in the simulation.

[23–25] examined how to measure the scatter fraction. Fig. 2shows the geometry used to measure scatter radiation in this study.

To generate scatter radiation for estimating the scatter fraction in our simulation study, a poly(methyl methacrylate) (PMMA) phantom was placed on the detector and then Pb was placed on the PMMA phantom. The scatter radiation was produced when an incident X-ray penetrated the PMMA phantom. If the incident X-ray was blocked perfectly by the Pb, then the area on the image in the location of the Pb is caused by only scatter radiation (I_s). Because of the geometry of the setup used in this study, only I_s could be calculated; it was difficult to evaluate only primary radiation (I_p). However, an image is formed I_p and I_s generated in the PMMA phantom ($I_p + I_s$). Therefore, the scatter fraction is calculated as follows [22]:

$$\text{Scatter Fraction} = \frac{I_s}{I_p + I_s} \times 100[\%]$$

Evaluation of image quality of the novel system: contrast

To investigate the relationship between scatter fraction and the image quality of the novel system, we calculated the image contrast by using a simulated phantom [26] made of PMMA and Al, where the PMMA represented a typical adult abdomen in Asian countries and the Al represented the vertebrae (Fig. 3).

The image contrast was calculated using the following formula [27]:

$$\text{Contrast} = \frac{|\text{ROI}_{\text{Al}} - \text{ROI}_{\text{PMMA}}|}{\text{ROI}_{\text{PMMA}}},$$

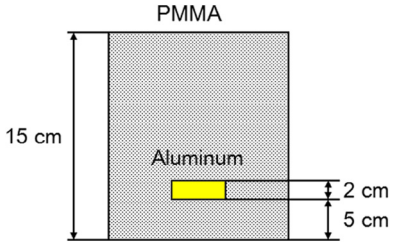

Figure 3. Simulated phantom used to evaluate image contrast. The PMMA represents a typical adult abdomen and the Al represents the vertebrae.

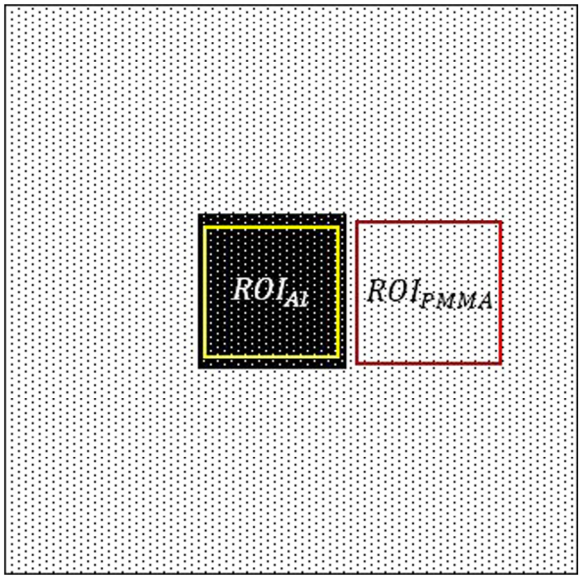

Figure 4. Schematic illustration of the regions of interest (ROI) used to calculate the image contrast.

where ROI_{Al} is the region of interest for Al and is the scatter radiation component measured under the Al and ROI_{PMMA} is the region of interest for PMMA and is the sum of the primary and scatter radiation components (Fig. 4). The ROIs were 10×10 pixels.

Results

Fig. 5shows the images from the simulations of no grid, parallel grid (8:1), and simulation #3 of the novel FPD system.

Fig. 6shows the scatter fraction as a function of increasing tube voltage for each simulated condition; the PMMA phantom used for these simulations was 10 cm thick. The structures, i.e., pixel size, thickness of the Pb, and the effective area of each pixel, of the no-grid system, parallel grid system, and simulation #1 of the proposed system were identical. However, the structures of simulations #1, #2, and #3 of the proposed system were different, as shown in Table 1. The no-grid scatter fraction was approximately 25% over the entire tube voltage range; when the parallel grid was between the PMMA phantom and the detector, the scatter fraction decreased to approximately 15%; and the scatter fraction for simulation #1 of the FPD system was ~11%. However, for the latter case, as the tube voltage increased, the scatter fraction also increased, so the performance of the novel system was inferior to that of the parallel grid in the tube voltage range of 80–120 kV. In simulation #2, we increased the thickness of the Pb from 10 to 20 μm, so the scatter fraction was less than that for simulation #1. The performance of simulation #2 of the novel system was superior to that of the parallel grid for tube voltages up to 80 kV, but there were no differences in performance between the two systems for tube voltages over 100 kV. Finally, for simulation #3, we kept the thickness of the Pb the same as in simulation #2 (20 μm) and the effective area the same as in simulation #1 (143 μm × 143 μm), but increased the total dimension of the pixels from 153 μm × 153 μm in simulation #2 to 163 μm × 163 μm. The scatter fraction of simulation #3 of the novel system was lower than that of the parallel grid and simulations #1 and #2 for the entire tube voltage range of 40–120 kV.

Fig. 7shows the scatter fraction for the simulated no-grid and parallel grid systems and simulation #3 of the novel system for which a 20-cm-thick PMMA phantom was used. Overall, the scatter fraction for the no-grid system with 20-cm-thick PMMA was

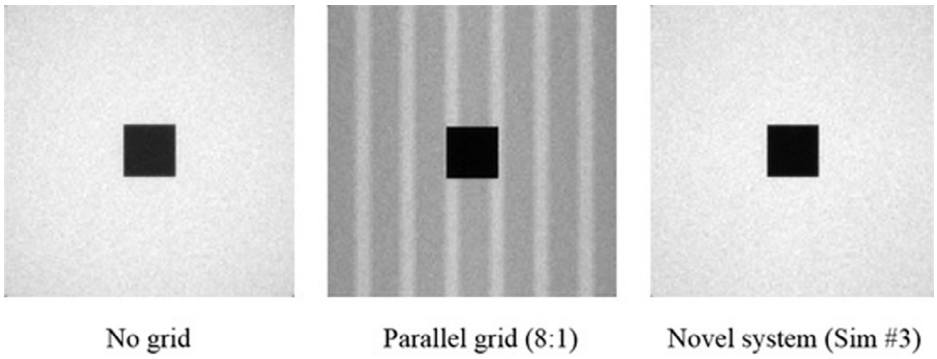

Figure 5. Images from the simulation of three different systems acquired at a tube voltage of 40 kV.

approximately twice that of the no-grid system with a 10-cm-thick PMMA. Only simulation #3, which had the best performance with the 10-cm-thick PMMA, was used in this simulation and its performance was superior to that of the parallel grid in the entire tube voltage range of 40–120 kV.

Fig. 8shows that the image contrast of the novel system was superior to that of the no-grid system for the entire tube voltage range, and that the image contrast decreased as the tube voltage increased for both the systems.

Discussion

In this paper, we presented a simulation study of the proposed novel FPD for removing scatter radiation. To evaluate the performance of the detector, we simulated the scatter fraction for a no-grid system, a parallel grid system, and the proposed system with three sets of specifications. In addition, we investigated the image contrast to determine the image quality of the novel system.

Kalender [28] found that the scatter fraction was approximately 40–60% in the energy range used in diagnostic radiology (0–150 keV) when the water phantom was 10 cm thick, the field size was 20 cm × 20 cm, and the scintillation material was CsI (60 mg/cm^2). Our study found that the scatter fractions for no-grid systems with 10- and 20-cm-thick PMMA phantoms were approximately 25% and 50%, respectively. Thus, doubling the thickness of the PMMA phantom doubled the scatter fraction, a result similar to that of the previous study [28]. The incident mean photon energy used in our study ranged from 34.3 to 68.4 keV (tube voltage: 40–120 kV) [20]. The scatter fraction found in the previous study [28] for the same incident energy and PMMA phantom thickness was approximately 40–50%, which is higher than that found by our study because of the difference in field size, i.e., 2 cm × 2 cm in our study vs. 10 cm × 10 cm in Kalender [28]. In addition, Kalender [28] found that the scatter fraction decreased approximately 50% when the field size decreased from 100 to 25 cm^2 at an incident energy of 60 keV.

In another study [29], the scatter fraction of an 8:1 ratio parallel grid system was approximately 45% of that of a no-grid system. In our study, the simulated 8:1 ratio parallel grid removed approximately 40% of the scatter radiation compared with the no-grid system for both the 10- and the 20-cm-thick PMMA phantoms; our scatter fraction results were similar to those of Tanaka et al. [29].

To investigate the feasibility of the novel FPD system, we optimized its structure with respect to detector specifications and the purpose of the radiological examination. First, noise resembling a Moiré pattern [30,31] appeared on the simulated images of the parallel grids (Fig. 5). To avoid this problem in clinical situations, a grid can be moved rapidly in front of the detector; however, one study reported that the noise remained on the image despite the moving grid [8]. Our proposed system uses a Pb net-like structure to match the ineffective area on the TFT layer. The shadow of the Pb structure does not appear on the image and the scatter radiation is removed.

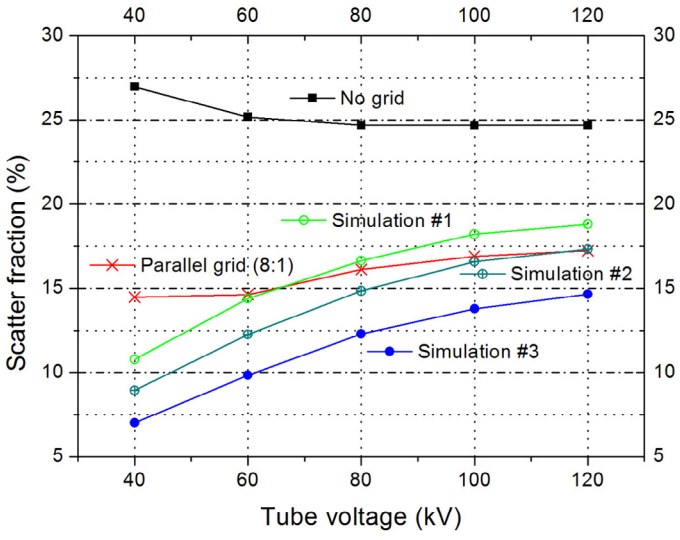

Figure 6. Scatter fraction for all simulated conditions (no grid, parallel grid, and simulations #1, #2, and #3 of the novel system) using a 10-cm-thick PMMA.

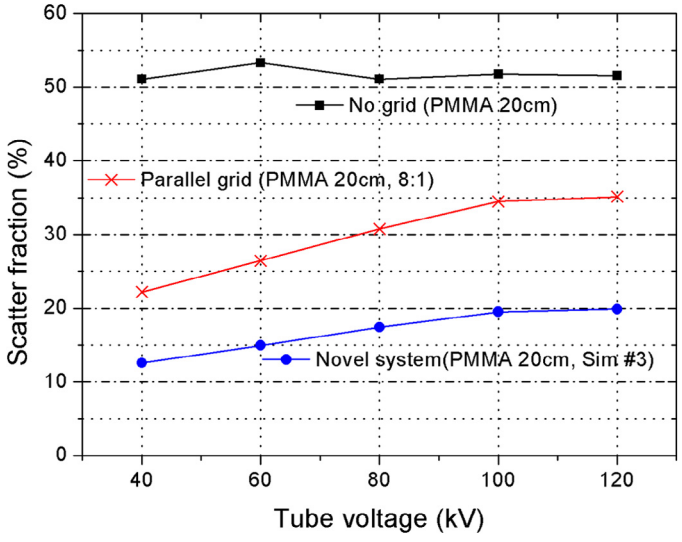

Figure 7. Scatter fraction for simulated no-grid and parallel grid systems and simulation #3 of the novel system using 20-cm-thick PMMA.

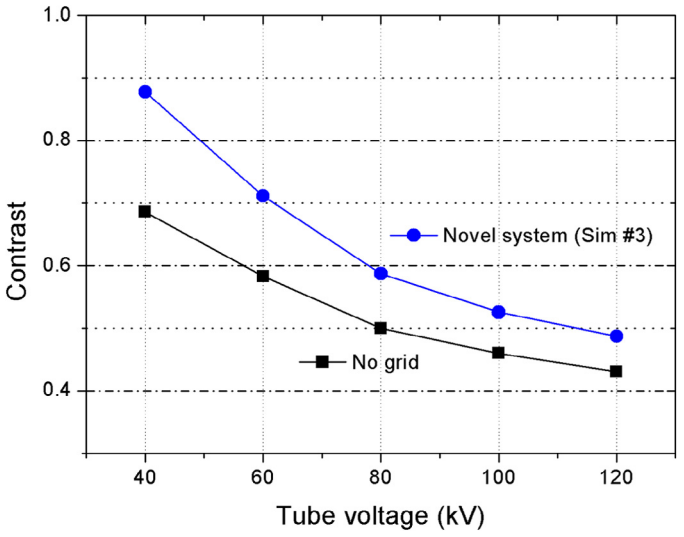

Figure 8. Image contrast for no-grid system and simulation #3 of the novel FPD system.

In simulation #1 of our proposed FPD system, the scatter fraction was superior to that of the parallel grid in the tube voltage range of 40–60 kV; however, as the tube voltage increased above 60 kV, the performance of the novel system decreased. In the tube voltage range of 80–100 kV, the performance of the novel system deteriorated to become worse than that of the parallel grid system because the specifications of the simulated Pb structure in the substrate layer were the same as those of the common parallel grid. The grid ratio of the novel system (horizontal 4:1, vertical 4:1) was the same as that of the parallel grid (8:1), but the Pb in the novel system that was to match the ineffective area on the TFT layer (10 μm thick) was approximately five times thinner than that in the parallel grid system (10 vs. 49 μm). Therefore, the generated scatter radiation increased as the energy of the incident X-rays increased, so simulation #1 of the novel system was less effective.

To improve the performance of the novel system, simulation #2 was conducted using thicker Pb (20 μm) than that used in simulation #1; consequently, the scatter radiation was approximately 12% less than that of simulation #1 and the performance was superior to that of the parallel grid in the tube voltage range of 40–80 kV. However, after the tube voltage reached 100 kV, the performance of the novel system was almost the same as that of the parallel grid. The efficacy of the thicker Pb decreased probably because it blocked the effective area on each pixel.

Pixel dimensions vary according to the manufacturer of the detector [32]. Thus, in simulation #3, the whole pixel size was increased to avoid blocking the effective area on the TFT layer. We kept the effective area the same (143 μm × 143 μm) as that in simulation #1 but the thickness of the Pb was doubled (20 μm). Thus, the scatter fraction of simulation #3 was approximately 28% less than that of simulation #1, and the performance of simulation #3 was superior to that of the parallel grid in the entire tube voltage range (40–120 kV). In simulation #2, the ratio of the blocked dimensions to the effective area was approximately 14%. The scatter fractions of simulations #2 and #3, in which the thickness of the Pb was the same but the dimensions of the effective areas were different, differed by approximately 16%. Therefore, the difference in performance between the two simulations is probably due to the different effective areas on the TFT layer.

The performance of the proposed FPD system varied with respect to the change in the structure from simulation #1 to #3. The structure of simulation #1 was good for low-tube-voltage conditions; thus, this structure would be effective for mammography, which uses a lower tube voltage. Simulations #2 and #3 had low scatter fractions with higher tube voltage, so these structures can be used for examinations that use a high tube voltage, such as chest radiographs.

A grid usually is used to reduce scatter radiation in most clinical situations, except when the upper or lower extremities. Thus, we investigated the performance of our novel system with a 20-cm-thick PMMA phantom and found that the scatter fraction and performance were similar to those of the system with a 10-cm-thick PMMA phantom. In addition, the performance of the novel system was superior to that of the parallel grid; therefore, the novel system might be useful in clinical situations in which there is a great amount of scatter radiation. Furthermore, our system had better image contrast than a no-grid system. Therefore, by reducing scatter radiation, the proposed system acquires better quality images.

The results of our study indicate that if the FPD system with a Pb net-like structure in the substrate layer is developed according to the specifications of the detector, the purpose of the radiological examination, and the tube voltage range, a better quality image can be obtained, even without using a conventional grid. However, this study has one limitation, i.e., the performance of the novel system was evaluated using only the scatter fraction and image contrast. To use this system in clinical situations, it should be evaluated using another method, such as with a Bucky factor, that identifies the relationship between patient dose and image quality. Furthermore, the image quality should be evaluated in terms of noise, e.g., via the contrast-to-noise ratio or the signal-to-noise ratio. Therefore, future study on our novel FPD system will use not only simulation but also hardware based on the foundation established in this study and these early-stage results.

Conclusion

If the structure of the novel FPD system with a Pb net-like structure is optimized with respect to the specifications of a specific detector, the purpose of the examination, and the energy range used, it can remove scatter radiation and can be used in diagnostic radiology.

Acknowledgment

This study was supported by a grant (K1422651) from the Institute of Health Science, Korea University, and the concept of this study has a patent pending (PCT/KR2015/001771).

References

[1] Chan H-P, Doi K. Physical characteristics of scattered radiation and the performance of antiscatter grids in diagnostic radiology. Radiographics 1982;2(3):378–406.
[2] Chan H-P, Doi K. Investigation of the performance of antiscatter grids: Monte Carlo simulation studies. Phys Med Biol 1982;27(6):785–803.
[3] International Commission on Radiological Protection. Statement from the 1985 Paris meeting of the International Commission on Radiological Protection. Ann ICRP 1985;15:32. Pub. 45.
[4] Seo D, Jang S, Kim J, Kim J, Sung D, Kim H, et al. A comparative assessment of entrance surface doses in analogue and digital radiography during common radiographic examinations. Radiat Prot Dosim 2014;158(1):22–7.
[5] Chan H-P, Higashida Y, Doi K. Performance of antiscatter grids in diagnostic radiology: experimental measurements and Monte Carlo simulation studies. Med Phys 1985;12(4):449–54.
[6] Riebel FA. The Moiré effect in radiography. Am J Roentgenol 1972;115(3):641–3.
[7] Cesar LJ, Schueler BA, Zink FE, Daly TR, Taubel JP, Jorgenson LL. Artefacts found in computed radiography. Br J Radiol 2001;74(878):195–202.
[8] Lin C-Y, Lee WJ, Chen SJ, Tsai CH, Lee JH, Chang CH, et al. A study of grid artifacts formation and elimination in computed radiographic images. J Digit Imaging 2006;19(4):351–61.
[9] Kim DS, Lee S. Grid artifact reduction for direct digital radiography detectors based on rotated stationary grids with homomorphic filtering. Med Phys 2013;40(6):061905.

[10] Okamura T, Tanaka S, Koyama K, Norihumi N, Daikokuya H, Matsuoka T, et al. Clinical evaluation of digital radiography based on a large-area cesium iodide-amorphous silicon flat-panel detector compared with screen-film radiography for skeletal system and abdomen. Eur Radiol 2002;12(7):1741–7.
[11] Beutel J, Kundel HL, Van Metter RL. Handbook of medical imaging. Volume 1: physics and psychophysics. Bellingham, WA: SPIE Press; 2000.
[12] Seibert JA. Flat-panel detectors: how much better are they? Pediatr Radiol 2006;36(2):173–81.
[13] Goldman LW. Specifications, performance evaluation, and quality assurance of radiographic and fluoroscopic systems in the digital era. Medical Physics Publishing 2004;177–228.
[14] Hamers S, Freyschmidt J. Digital radiography with an electronic flat-panel detector: first clinical experience in skeletal diagnostics. Medicamundi 1998;42:2–6.
[15] Nagarkar VV, Gupta TK, Miller SR, Klugerman Y, Squillante MR, Entine G. Structured CsI (Tl) scintillators for X-ray imaging applications. IEEE Trans Nucl Sci 1998;45(3):492–6.
[16] Kim BJ, Cha BK, Jeon H, Chi YK, Cho G. A study on spatial resolution of pixelated CsI (Tl) scintillator. Nucl Instrum Meth A 2007;579(1):205–7.
[17] Rowlands JA, Zhao W, Blevis IM, Waechter DF, Huang Z. Flat-panel digital radiology with amorphous selenium and active-matrix readout. Radiographics 1997;17(3):753–60.
[18] Chotas HG, Dobbins IIIJT, Ravin CE. Principles of digital radiography with large-area, electronically readable detectors: a review of the basics. Radiology 1999;210(3):595–9.
[19] Pelowitz DB. MCNPX User's Manual, version 2.6.0. Los Alamos, NM: Los Alamos National Laboratory; 2008.
[20] The Institute of Physics and Engineering in Medicine Report 78. York, UK: IPEM; 1997.
[21] DeMarco JJ, Wallace RE, Boedeker K. An analysis of MCNP cross-sections and tally methods for low-energy photon emitters. Phys Med Biol 2002;47(8):1321.
[22] Dick CE, Soares CG, Motz JW. X-ray scatter data for diagnostic radiology. Phys Med Biol 1978;23(6):1076–85.
[23] Chan H-P, Doi K. The validity of Monte Carlo simulation in studies of scattered radiation in diagnostic radiology. Phys Med Biol 1983;28(2):109–29.
[24] Schmidt RA, Chan H-P, Kodera Y, Doi K, Chen CT. Evaluation of cassette performance: physical factors affecting patient exposure and image contrast. Radiology 1983;146(3):801–6.
[25] Boone JM. Scatter correction algorithm for digitally acquired radiographs: theory and results. Med Phys 1986;13(3):319–28.
[26] Oishi Y, Sano Y, Yoshida KI, Iwanaga H, Yasui KI, Fujimoto K, et al. Study of image quality (contrast) and reduction of patient dose by using heavy metal filters. Jpn J Radiol Technol 2002;8(1):109–14.
[27] Dobbins JT, Samei E, Chotas HG, Warp RJ, Baydush AH, Floyd CE Jr, et al. Chest radiography: optimization of X-ray spectrum for cesium iodide–amorphous silicon flat-panel detector 1. Radiology 2003;226(1):221–30.
[28] Kalender W. Monte Carlo calculations of x-ray scatter data for diagnostic radiology. Phys Med Biol 1981;26(5):835–49.
[29] Tanaka N, Naka K, Saito A, Morishita J, Toyofuku F, Ohki M, et al. Investigation of optimum anti-scatter grid selection for digital radiography: physical imaging properties and detectability of low-contrast signals. Radiol Phys Technol 2013;6(1):54–60.
[30] Goodman JW, Gustafson SC. Introduction to Fourier optics. Opt Eng 1996;35(5):1513.
[31] Kafri O, Glatt I. Surface Topography and Spinal Deformity: Proceedings of the 6th International Symposium, September 19–20, 1990. Estoril, Jena: Gustav Fischer; 1992.
[32] Kotter E, Langer M. Digital radiography with large-area flat-panel detectors. Eur Radiol 2002;12(10):2562–70.